

Magnetic Raman continuum in single crystalline $\text{H}_3\text{LiIr}_2\text{O}_6$

Shenghai Pei,^{1,2,*} Liang-Long Huang,^{2,*} Gaomin Li,^{3,2} Xiaobin Chen,⁴ Bin Xi,⁵ XinWei Wang,³ Youguo Shi,^{6,7} Dapeng Yu,² Cai Liu,² Le Wang,^{2,†} Fei Ye,² Mingyuan Huang,^{2,8,‡} and Jia-Wei Mei^{2,§}

¹Department of Physics, Harbin Institute of Technology, Harbin 150001, China

²Shenzhen Institute for Quantum Science and Engineering, and Department of Physics, Southern University of Science and Technology, Shenzhen 518055, China

³School of Advanced Materials, Shenzhen Graduate School Peking University, Shenzhen 518055, P. R. China

⁴School of Science, Harbin Institute of Technology, Shenzhen 518055, China

⁵College of Physics Science and Technology, Yangzhou University, Yangzhou 225002, China

⁶Institute of Physics, Chinese Academy of Sciences, Beijing 100190, China

⁷School of Physical Sciences, University of Chinese Academy of Sciences, Beijing 100190, China

⁸Shenzhen Key Laboratory of Quantum Science and Engineering, Shenzhen 518055, PR China.

(Dated: June 11, 2019)

Recently $\text{H}_3\text{LiIr}_2\text{O}_6$ has been reported as a spin-orbital entangled quantum spin liquid (QSL) [K. Kitagawa et al., Nature **554**, 341 (2018)], albeit its connection to Kitaev QSL has not been yet identified. To unveil the related Kitaev physics, we perform the first Raman spectroscopy studies on single crystalline $\text{H}_3\text{LiIr}_2\text{O}_6$ samples. We implement a soft chemical replacement of Li^+ with H^+ from $\alpha\text{-Li}_2\text{IrO}_3$ single crystals to synthesize the single crystal samples of the iridate second generation $\text{H}_3\text{LiIr}_2\text{O}_6$. The Raman spectroscopy can be used to diagnose the QSL state since the magnetic Raman continuum arises from a process involving pairs of fractionalized Majorana fermionic excitation in a pure Kitaev model. We observe a broad dome-shaped magnetic continuum in $\text{H}_3\text{LiIr}_2\text{O}_6$, in line with theoretical expectations for the two-spin process in the Kitaev QSL. Our results establish the close connection to the Kitaev QSL physics in $\text{H}_3\text{LiIr}_2\text{O}_6$.

Introduction. – The search for quantum spin liquid (QSL) state has been a currently active and challenging topic in the condensed matter physics [1–12]. The spin degree of freedom in QSL does not freeze to display any magnetic order even at zero temperature, but highly entangles with each other [13–18]. In the early theoretical studies, the exact solvable Kitaev honeycomb spin model [13] built confidence about the existence of QSL in a simple spin interacting system; furthermore, it has been currently initialing the materialization of the Kitaev QSL in the experiments [19–21]. With the help of the intertwining between magnetism, spin-orbital coupling, and crystal field, Ir^{4+} oxides and a Ru^{3+} chloride with a d^5 electronic configuration are promising to materialize the Kitaev model, e.g., $\alpha\text{-A}_2\text{IrO}_3$ ($A=\text{Na}, \text{Li}$) [22–24] and $\alpha\text{-RuCl}_3$ [25].

Due to other non-Kitaev interactions, magnetic orders appears in $\alpha\text{-A}_2\text{IrO}_3$ ($A=\text{Na}, \text{Li}$) and $\alpha\text{-RuCl}_3$ at low temperatures [22, 26, 27]. The suppression of magnetic ordering in $\alpha\text{-A}_2\text{IrO}_3$ ($A=\text{Na}, \text{Li}$) and $\alpha\text{-RuCl}_3$ has been attempted by applying magnetic field [28, 29], high pressure [30–32], and chemical modification [12, 33]. For the chemical modification of $\alpha\text{-Li}_2\text{IrO}_3$, a QSL state ground was recently established in the second generation of two-dimensional honeycomb iridates $\text{H}_3\text{LiIr}_2\text{O}_6$ [12, 33]. No sign of magnetic order, but signatures of local low-energy excitations are observed in $\text{H}_3\text{LiIr}_2\text{O}_6$, down to low temperatures in the magnetic susceptibility, specific heat, and NMR measurements [12]. $\text{H}_3\text{LiIr}_2\text{O}_6$ has immediately caught lots of theoretical investigation to explore the connection to the Kitaev QSL physics [34–38], and the randomness of H positions was also discussed as play-

ing an important role in stabilizing the QSL state [35, 36]. Currently, however, no spectroscopic information exists regarding the spin excitations and the possibility of spin fractionalization in $\text{H}_3\text{LiIr}_2\text{O}_6$.

In this Letter, we report our attempts to diagnose the spin liquid signature in the single crystalline $\text{H}_3\text{LiIr}_2\text{O}_6$ using the Raman spectroscopy methods. Single crystals of $\alpha\text{-Li}_2\text{IrO}_3$ are soaked in 4 mol/L H_2SO_4 aqueous solution for the soft chemical replacement of Li^+ with H^+ . As well as single crystals of the target second generation of iridate $\text{H}_3\text{LiIr}_2\text{O}_6$, we obtain the third iridate generation with the hypothesized formula $\text{H}_5\text{LiIr}_2\text{O}_6$. We carry out the X-ray photoelectron spectroscopy (XPS) measurements, and confirm that $\text{H}_3\text{LiIr}_2\text{O}_6$ has the same Ir^{4+} oxidation state as $\alpha\text{-Li}_2\text{IrO}_3$, while $\text{H}_5\text{LiIr}_2\text{O}_6$ has lower oxidation state Ir^{3+} . Submillimetre-size crystals are available for the Raman spectroscopy, that is capable of detecting magnetic excitations [39–41], even the spin fractionalizations signaled by the magnetic Raman continuum in the Kitaev-type compounds [31, 32, 42–44]. We observe a broad two-spin process continuum in the dynamical Raman susceptibility for $\text{H}_3\text{LiIr}_2\text{O}_6$, in a good agreement with the theoretically expected scattering from a pure Kitaev model [45]. Our results demonstrate Raman spectroscopic signatures of the fractionalized excitation for the Kitaev QSL state in $\text{H}_3\text{LiIr}_2\text{O}_6$.

Single crystal synthesis and experimental setup. – We implement the soft chemical replacement of Li^+ with H^+ in the iridate first generation $\alpha\text{-Li}_2\text{IrO}_3$ single crystals. We obtain single crystals of different generations of honeycomb iridate oxides, depending the growth condition, especially reaction (soaking) time. For the growth

of α - Li_2IrO_3 single crystal, we adopted the similar setup as described in Ref. [46] with iridium metal (powder, 99.99%) and lithium (granule, 99.99%) used as starting materials. The whole setup was placed in a preheated furnace of 200 °C heated to 1020 °C and dwelled for 10 days. For cation exchange, α - Li_2IrO_3 single crystals were added into in a 25 ml Teflon-lined steel autoclave with 20 ml H_2SO_4 aqueous solution (4 mol/L).

The XPS investigations were carried out on Thermo Fisher ESCALAB 250Xi using monochromated Al K α radiation at room temperature, and the electron flood gun was turned on to eliminate electric charging effect in our insulating samples. The binding energy in XPS was calibrated by 1s spectra of carbon. XRD measurements were conducted on Rigaku Smartlab 9KW using Cu K α radiation at room temperature.

The Raman spectra were measured in the quasi-back-scattering geometry, with light polarized in the basal plane. The experiments were performed on our home-built system using a HORIBA iHR550 spectrometer and the 632.8 nm excitation line of a He-Ne laser. The power of the laser was kept low enough (about 100 μW) to prevent from heating and damaging samples. We use 1200 grooves/mm grating to get the high resolution. Since the light scattering intensity is weak, we set the integral time to 1800 s. The samples were placed in a He-flow cryostat which evacuated to 2.0×10^{-6} Torr. The sample temperatures were calibrated according to the intensity ratio of anti-Stokes and Stokes phonon peaks.

Sample characterizations. – Single crystals of α - Li_2IrO_3 have different appearances, e.g., the flake and

pyramid shapes, probably due to different stacking patterns of LiIr_2O_6 layers. We find that the pyramid-shaped α - Li_2IrO_3 have more ordered stacking pattern, however, the flake-shaped crystals are easily accessible for the soft chemical replacement as the present study in this work. Fig. 1 (a) is the image for typical single crystals of three generations of the iridate oxides. The parent generation α - Li_2IrO_3 (the flake crystal) displays the black appearance. The second generation ($\text{H}_3\text{LiIr}_2\text{O}_6$) has the reddish black color, and the third generation (hypothesized formula $\text{H}_5\text{LiIr}_2\text{O}_6$) has the lustrous red appearance. During the soft-chemical-ion-exchange reaction (about 70 min), the interlayer Li^+ will be replaced by H^+ , and we can get the target iridate second generation $\text{H}_3\text{LiIr}_2\text{O}_6$. With longer soaking time (about 3 hours), more Hydrogen atoms intercalate into the inter-layers of $[\text{LiIr}_2\text{O}_6]$ layers, and we get the crystals of the third generation $\text{H}_5\text{LiIr}_2\text{O}_6$. While α - Li_2IrO_3 and $\text{H}_5\text{LiIr}_2\text{O}_6$ is very stable, $\text{H}_3\text{LiIr}_2\text{O}_6$ may react with the vapour in the air.

Figure. 1 (b) is the powder X-ray diffraction (PXRD) result for three generations of iridate oxides. Apparently, they have very similar overall PXRD patterns since the acid treatment have caused a mild change in the constitution of the LiIr_2O_6 layers, and only the ions situated in-between the layers are changed. The intense basal reflection 2θ shifts up from α - Li_2IrO_3 (18.36°) to $\text{H}_3\text{LiIr}_2\text{O}_6$ (19.52°), and then down to $\text{H}_5\text{LiIr}_2\text{O}_6$ (18.85°), corresponding to the interlayer distance 4.828 Å, 4.544 Å and 4.704 Å, respectively. Strong anisotropic broadening of the reflections in the XRD-pattern revealed heavy stacking faulting of the samples. Fig. 1 (c) is the typical Raman result for the three generations at a room temperature. The Raman intensity of $\text{H}_5\text{LiIr}_2\text{O}_6$ rescales by multiplying by 1/2. During the crystal synthesis, we use the Raman spectra to monitor the soaking process of our samples.

We implement XPS to verify the oxidation state of iridium ions in the three generations. As shown in Fig. 1 (d), three generations have very similar Ir $4f$ XPS spectra, indicating the similar local electronic environment of IrO_6 . The shift of the binding energy of Ir $4f$ implies the changes of oxidation state of Ir, and lower binding energy represents lower valance state. The mild change can be seen from α - Li_2IrO_3 to $\text{H}_3\text{LiIr}_2\text{O}_6$ by comparing the position of $4f_{5/2}$ and $4f_{7/2}$ energy level, indicating the same electronic configuration of Ir^{4+} . $\text{H}_5\text{LiIr}_2\text{O}_6$ has a significant lower binding energy (about 0.7 eV). According to Ir-based compounds in the database[47], Ir^{3+} and Ir^{4+} usually have a difference of the binding energy about 0.5 eV. Comparing Ir^{4+} in α - Li_2IrO_3 and $\text{H}_3\text{LiIr}_2\text{O}_6$, we have Ir^{3+} in IrO_6 octahedron in $\text{H}_5\text{LiIr}_2\text{O}_6$. Ir^{3+} has the $3d^6$ electronic configurations without partially occupied orbitals, and hence no magnetism. This explains the negligible magnetic Raman continuum in $\text{H}_5\text{LiIr}_2\text{O}_6$

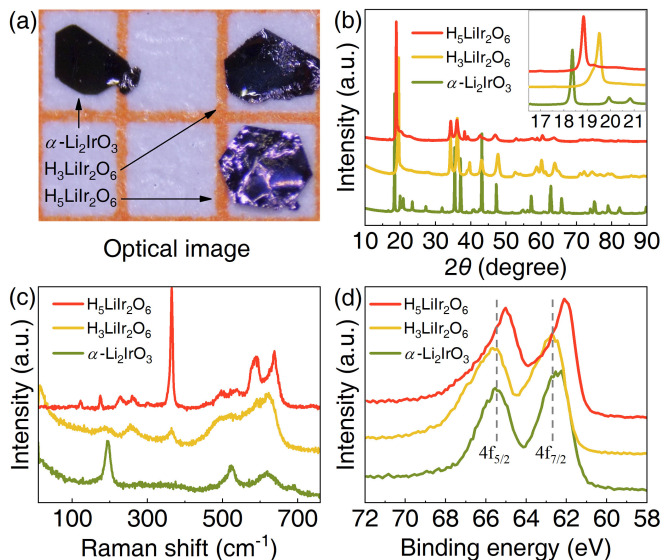


FIG. 1. (a) Image of single crystals for α - Li_2IrO_3 , $\text{H}_3\text{LiIr}_2\text{O}_6$ and $\text{H}_5\text{LiIr}_2\text{O}_6$, respectively. The yellow background grid is $1 \times 1 \text{ mm}^2$. To characterize three iridate generations at a room temperature, we have measured three PXRD patterns in (b), Raman spectra in (c), and XPS in (d).

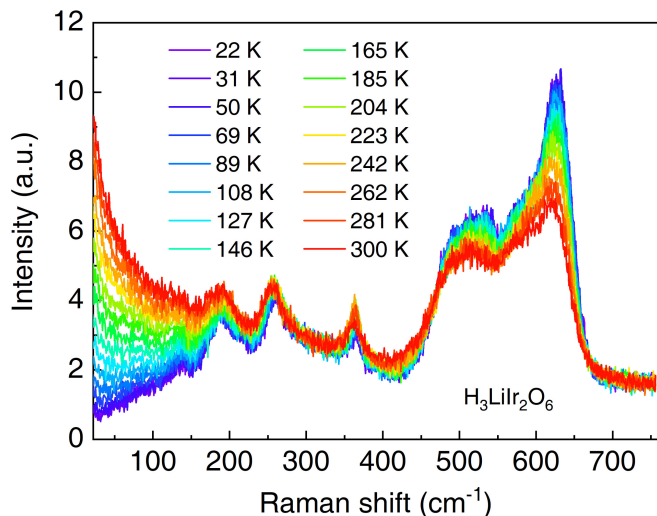


FIG. 2. Evolution of the Raman spectra at different temperatures in $\text{H}_3\text{LiIr}_2\text{O}_6$. The spectra composes sharp phonon peaks and the broad magnetic continuum.

as shown in Fig. 1 (c) and Fig. 3.

Evolution of Raman spectra – Figures. 2 is the evolution of Raman spectra of $\text{H}_3\text{LiIr}_2\text{O}_6$ at different temperatures. Comparing with our $\alpha\text{-Li}_2\text{IrO}_3$ results [32], we can assign the sharp phonon modes by assuming that $\text{H}_3\text{LiIr}_2\text{O}_6$ has the same space group (#12, C2/m) as $\alpha\text{-Li}_2\text{IrO}_3$. Three modes at 364.0 and 630.8 cm^{-1} are assigned as A_g modes, the mode at 131.9 cm^{-1} is assigned as B_g mode, and four modes at 189.6, 259.9, 490.0 and 541.0 cm^{-1} are assigned as $A_g + B_g$ modes which are nearly doubly degenerate. 131.9 and 189.6 cm^{-1} modes are the Ir-Ir out-of-phase motions along the out-of-plane and in-plane directions, respectively. The 259.9 cm^{-1} mode is the twist of Ir-O-Ir-O plane, the 364.0 cm^{-1} mode is the relative twist of between the upper and lower oxygen triangles. The 490 cm^{-1} mode is related to the Ir-O-Ir-O plane shearing, and the 541.0 cm^{-1} mode is the breathing mode of Ir-O-Ir-O ring. The A_g mode at 630.8 cm^{-1} can be assigned as the symmetrical breathing mode between the upper and lower oxygen layers. Several weak phonon peaks at around 155, 220, 325 and 600 cm^{-1} become visible at low temperatures in $\text{H}_3\text{LiIr}_2\text{O}_6$, and these modes don't appear in $\alpha\text{-Li}_2\text{IrO}_3$ [32]. We notice that Raman phonon modes in $\text{H}_3\text{LiIr}_2\text{O}_6$ in this work and $\alpha\text{-Li}_2\text{IrO}_3$ [32] are quite similar to those in other Kitaev materials, e.g. $\alpha\text{-RuCl}_3$ [31, 42] and β - and $\gamma\text{-Li}_2\text{IrO}_3$ [43], suggestive of similar local crystal RuCl_6 and IrO_6 octahedral structures.

Besides the phonon modes, we observe a strong continuum background with increasing intensity as increasing temperatures particularly for low Raman frequencies (Fig. 2). We attribute such a continuum background as the magnetic Raman scattering as observed in $\alpha\text{-RuCl}_3$ [42] and β - and $\gamma\text{-Li}_2\text{IrO}_3$ [43] due to spin fraction-

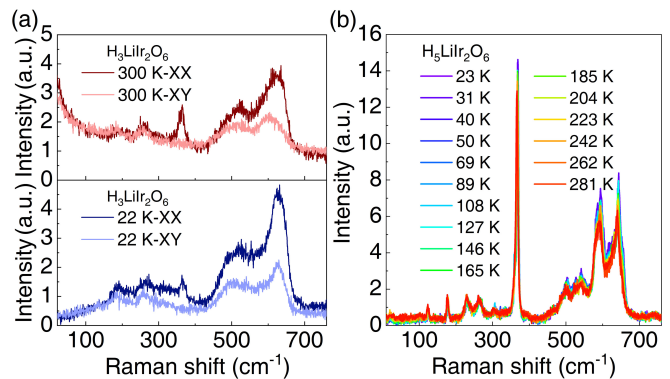


FIG. 3. (a) The polarized Raman spectra at 300 K (upper) and 20 K in $\text{H}_3\text{LiIr}_3\text{O}_6$. (b) Evolution of the Raman spectra at different temperatures in $\text{H}_5\text{LiIr}_2\text{O}_6$. As a control experiment, there is no magnetic Raman continuum at all.

alized excitations. $\text{H}_3\text{LiIr}_2\text{O}_6$ is a layered material and there are heavily stacking faults which may lead to broad phonon modes that could explain the continuum. However, the static structural disorder cannot produce the significant temperature dependence. Furthermore, the damped phonon scenario couldn't account for the Raman continuum according to the polarization dependence of the Raman spectra in $\text{H}_3\text{LiIr}_2\text{O}_6$ as shown in Fig. 3 (a). As a matter of fact, the weak polarization dependence of Raman spectra in $\text{H}_3\text{LiIr}_2\text{O}_6$ agrees well with theoretical calculations for the isotropic Kitaev model [48].

As a control experiments, Fig. 3 (b) is the evolution of Raman spectra in $\text{H}_5\text{LiIr}_2\text{O}_6$ at different temperatures. Actually, $\text{H}_5\text{LiIr}_2\text{O}_6$ would have similar stacking faults to $\text{H}_3\text{LiIr}_2\text{O}_6$ since they main difference in their synthesis is the soaking time of the soft chemical reaction. With increasing temperature, all phonon peaks in $\text{H}_5\text{LiIr}_2\text{O}_6$ change very mild, and there is not any continuum background at all at the whole temperature range, which is in contrast to the spectra of $\text{H}_3\text{LiIr}_2\text{O}_6$ in Fig. 2. On one hand, as a control experiment, the Raman spectra of $\text{H}_5\text{LiIr}_2\text{O}_6$ in Fig. 3 (b) implies that the continuum background of $\text{H}_3\text{LiIr}_2\text{O}_6$ in Fig. 2 is not due to the stacking faults, but has the magnetic origin. On the other hand, even if some regions of $\text{H}_3\text{LiIr}_2\text{O}_6$ (Ir^{4+}) turn into $\text{H}_5\text{LiIr}_2\text{O}_6$ (Ir^{3+}) due to the over soaking in the acid, they behave as handfull impurities and do not contribute to the magnetic Raman continuum.

According to the fluctuation-dissipation theorem, the Raman intensity $I(\omega)$ is proportional to the dynamical Raman susceptibility as $I(\omega) = [1 + n(\omega)]\chi''(\omega)$. Here $n(\omega)$ is the boson factor, and $\chi''(\omega)$ is the imaginary part of the correlation functions of Raman tensor $\tau(\mathbf{r}, t)$, $\chi(\omega) = \int_0^\infty dt \int d\mathbf{r} (-i) \langle [\tau(0, 0), \tau(\mathbf{r}, t)] \rangle e^{-i\omega t}$. To examine the the magnetic Raman susceptibility $\chi''(\omega)$ in $\text{H}_3\text{LiIr}_2\text{O}_6$ more explicitly, we remove phonon modes using the Gaussian-type line-shape. As a consequence, the obtained magnetic Raman susceptibility in $\text{H}_3\text{LiIr}_2\text{O}_6$

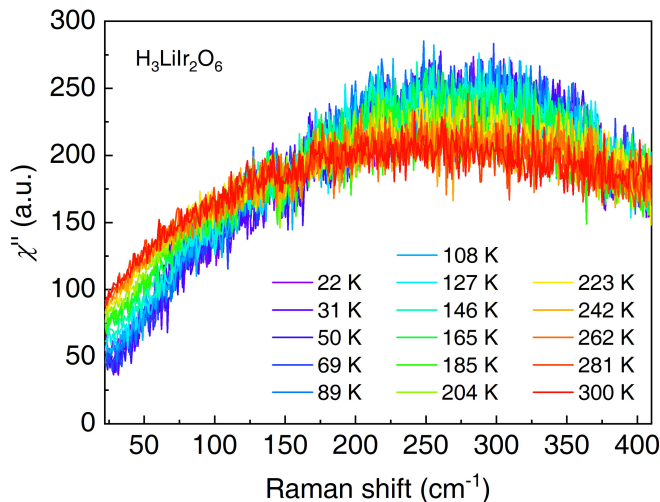


FIG. 4. Temperature dependent revolution of magnetic Raman continuum in the dynamical Raman susceptibility $\chi''(\omega)$ in $\text{H}_3\text{LiIr}_2\text{O}_6$.

displays a dome-shaped broad continuum at all temperatures, as shown in Fig. 4. With the temperature decreasing, the magnetic Raman continuum increases with the frequency between 150 cm^{-1} and 410 cm^{-1} , and decreases with the frequency less than 150 cm^{-1} . Thus the dome shape of the magnetic continuum is more remarkable at low temperatures. From the Raman intensity in Fig. 2, we can see that the magnetic continuum extends to higher frequencies at least up to 700 cm^{-1} . The phonon modes with the frequency between 410 cm^{-1} and 710 cm^{-1} are messy, and it is not easy to separate the phonon modes and magnetic continuum in the frequency region (between 410 cm^{-1} and 710 cm^{-1}). Therefore, we didn't show the subtracted magnetic Raman continuum with the frequency between 410 cm^{-1} and 710 cm^{-1} in Fig. 4. We can see that the magnetic continuum is weakly temperature dependent in this frequency region according to the Raman spectra in $\text{H}_3\text{LiIr}_2\text{O}_6$ in Fig. 2.

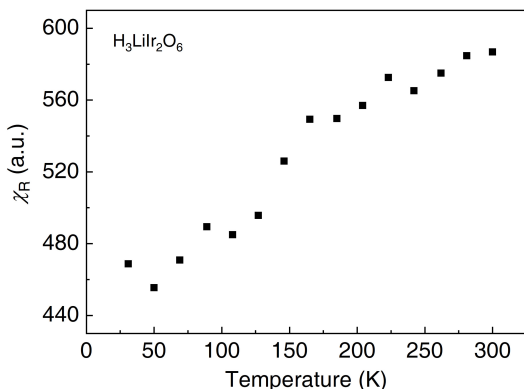


FIG. 5. Temperature dependent magnetic Raman susceptibility $\chi_R(T)$ in $\text{H}_3\text{LiIr}_2\text{O}_6$.

We extract the integrated Raman susceptibility χ_R in accordance with the Kramers-Kronig relation $\chi_R = \frac{2}{\pi} \int \frac{\chi''(\omega)}{\omega} d\omega$. To do the integration, we extrapolate the Raman conductivity $\frac{\chi''(\omega)}{\omega}$ in $\text{H}_3\text{LiIr}_2\text{O}_6$ to 0 cm^{-1} . The temperature dependent χ_R in $\text{H}_3\text{LiIr}_2\text{O}_6$ is plotted in Fig. 5, in which the integration is carried out from 0 cm^{-1} to 410 cm^{-1} , taking into account the fact that the magnetic Raman continuum with the frequency between 410 cm^{-1} and 710 cm^{-1} is weakly temperature dependent. The integrated Raman susceptibility χ_R in $\text{H}_3\text{LiIr}_2\text{O}_6$ essentially decreases monotonically as lowering the temperatures at least above 50 K , very different from that in $\alpha\text{-Li}_2\text{IrO}_3$ [32], where χ_R increases monotonically with temperature decreasing. It is worthy to mention that the temperature dependence of χ_R in $\text{H}_3\text{LiIr}_2\text{O}_6$ is similar to β - and $\gamma\text{-Li}_2\text{IrO}_3$ [43]. The integrated Raman susceptibility χ_R of $\alpha\text{-Li}_2\text{IrO}_3$ has a very similar temperature dependence behavior to $\alpha\text{-RuCl}_3$, *i.e.* increasing monotonically with temperature decreasing [32, 44]. More specifically, the inelastic light scattering in $\text{H}_3\text{LiIr}_2\text{O}_6$ and β - and $\gamma\text{-Li}_2\text{IrO}_3$ has different form from that in $\alpha\text{-RuCl}_3$ and $\alpha\text{-Li}_2\text{IrO}_3$, which deserves further detail investigations.

Discussions and conclusions – With the help of strong spin-orbit coupling, crystal field splitting and electronic correlation, the Kitaev materials have the effective spin-1/2 moment [19, 21]. The magnetic Raman tensor $\tau(\mathbf{r})$ in these systems can be expanded in powers of the effective spin-1/2 operators, $\tau^{\alpha\beta}(\mathbf{r}) = \tau_0^{\alpha\beta}(\mathbf{r}) + \sum_{\mu} K_{\mu}^{\alpha\beta} S^{\mu}(\mathbf{r}) + \sum_{\delta} \sum_{\mu\nu} M_{\mu\nu}^{\alpha\beta}(\mathbf{r}, \delta) S_{\mathbf{r}}^{\mu} S_{\mathbf{r}+\delta}^{\nu} + \dots$. The first term corresponds to Rayleigh scattering, the second and third terms correspond to the one-spin and two-spin process, respectively [39–41]. The complex tensors $K_{\mu}^{\alpha\beta}$ and $M_{\mu\nu}^{\alpha\beta}$ are determined by the strength of the spin-orbit couplings and the subtle coupling form of light to the spin system. If the one-spin process dominates the inelastic light scattering, the integrated Raman susceptibility χ_R is associated with the thermodynamic magnetic susceptibility χ , as demonstrated in $\alpha\text{-RuCl}_3$ [44] and $\alpha\text{-Li}_2\text{IrO}_3$ [32]. In β - and $\gamma\text{-Li}_2\text{IrO}_3$, the integrated Raman susceptibility χ_R^0 is associated with the magnetic-specific heat C_m multiplied by the temperature T , *i.e.*, $C_m T$ [43], indicating that the two-spin process dominates the magnetic Raman scattering.

The temperature dependence behavior of $\text{H}_3\text{LiIr}_2\text{O}_6$ is similar to that in β - and $\gamma\text{-Li}_2\text{IrO}_3$, therefore, two-spin process dominates in the magnetic Raman continuum in Fig. 4. In the putative Kitaev QSL, the magnetic Raman scattering of two-spin process directly probes the pairs of the Majorana fermions which are characterization of the elusive spin fractionalizations [48, 49]. Particularly, Knolle *et al.* have calculated the magnetic Raman scattering for the two-spin process, and our dome-shaped magnetic Raman continuum agrees very well with the simulated Raman response [48]. Therefore, our results

demonstrate the emergence of spin fractionalization, and establish a Kitaev QSL in $\text{H}_3\text{LiIr}_2\text{O}_6$. The theoretical simulated Raman response has a maximum at $1.5 J_k$ (where J_k is the Kitaev interaction for the effective spin-1/2 operators) [48]. Equating $1.5 J_K$ with the experimental maximum of continuum scattering of 40 meV yields $J_K = 26$ meV, in a good consistent with DFT estimations [35–37].

$\text{H}_3\text{LiIr}_2\text{O}_6$ have heavily stacking faults [12, 33], and theoretical investigations of have discussed the important role of the randomness to stabilize the Kitaev QSL [34–38]. However, Raman scattering is not sensitive to the local randomness, and our results didn't address the issue about the physics of disorder in quantum spin liquids. Knolle *et. al.* predicted a δ -function peak reflecting the local two-particle density of states of Majorana fermions in the presence of four vison fluxes [48]. Such a vison peak is not resolved in our Raman data due to the severely bad resolution at small wave numbers.

In conclusion, we perform the Raman spectroscopy studies of single-crystal $\text{H}_3\text{LiIr}_2\text{O}_6$ samples and observe a dome-shaped magnetic Raman continuum. Our results demonstrate the spin fractalization in $\text{H}_3\text{LiIr}_2\text{O}_6$, which is a defining feature of the Kitaev quantum spin liquid state.

Acknowledgments – J.W. M thanks L. Zhang for informative discussions, and Y.L. He and A. Ng for useful discussions on the XPS measurements. This work was supported by the Science, Technology and Innovation Commission of Shenzhen Municipality (Grant No.ZDSYS20170303165926217). M.H. was partially supported by the Science, Technology and Innovation Commission of Shenzhen Municipality (Grant No. JCYJ20170412152334605). F.Y. was partially supported by National Nature Science Foundation of China (Grant No. 11774143) and the Science, Technology and Innovation Commission of Shenzhen Municipality (Grant No. JCYJ20160531190535310). J.W.M was partially supported by the program for Guangdong Introducing Innovative and Entrepreneurial Teams (No. 2017ZT07C062)

* These two authors contribute to this work equally.

† wangl2018@mail.sustc.edu.cn

‡ huangmy@sustc.edu.cn

§ meijw@sustc.edu.cn

- [1] P. W. Anderson, “Resonating valence bonds: A new kind of insulator?” *Materials Research Bulletin* **8**, 153–160 (1973).
- [2] Philip W Anderson, “The Resonating Valence Bond State in La_2CuO_4 and Superconductivity.” *Science* **235**, 1196–8 (1987).
- [3] Leon Balents, “Spin liquids in frustrated magnets,” *Nature* **464**, 199 (2010).
- [4] Lucile Savary and Leon Balents, “Quantum spin liquids: a review,” *Reports on Progress in Physics* **80**, 016502 (2017).
- [5] Yi Zhou, Kazushi Kanoda, and Tai-Kai Ng, “Quantum spin liquid states,” *Rev. Mod. Phys.* **89**, 025003 (2017).
- [6] Y. Shimizu, K. Miyagawa, K. Kanoda, M. Maesato, and G. Saito, “Spin liquid state in an organic mott insulator with a triangular lattice,” *Phys. Rev. Lett.* **91**, 107001 (2003).
- [7] Emily A. Nytko, Joel S. Helton, Peter Müller, and Daniel G. Nocera, “A Structurally Perfect S=1/2 Metal-Organic Hybrid Kagome Antiferromagnet,” *Journal of the American Chemical Society* **130**, 2922–2923 (2008).
- [8] Zili Feng, Zheng Li, Xin Meng, Wei Yi, Yuan Wei, Jun Zhang, Yan-Cheng Wang, Wei Jiang, Zheng Liu, Shiyang Li, Feng Liu, Jianlin Luo, Shiliang Li, Guo qing Zheng, Zi Yang Meng, Jia-Wei Mei, and Youguo Shi, “Gapped Spin-1/2 Spinon Excitations in a New Kagome Quantum Spin Liquid Compound $\text{Cu}_3\text{Zn}(\text{OH})_6\text{FBr}$,” *Chinese Physics Letters* **34**, 077502 (2017).
- [9] Xiao-Gang Wen, “Discovery of fractionalized neutral spin-1/2 excitation of topological order,” *Chinese Physics Letters* **34**, 090101 (2017).
- [10] Yuan Wei, Zili Feng, Wiebke Lohstroh, Clarina dela Cruz, Wei Yi, Z. F. Ding, J. Zhang, Cheng Tan, Lei Shu, Yang-Cheng Wang, Jianlin Luo, Jia-Wei Mei, Zi Yang Meng, Youguo Shi, and Shiliang Li, “Evidence for a z_2 topological ordered quantum spin liquid in a kagome-lattice antiferromagnet,” (2017), [arXiv:1710.02991](https://arxiv.org/abs/1710.02991).
- [11] Zili Feng, Yuan Wei, Ran Liu, Dayu Yan, Yan-Cheng Wang, Jianlin Luo, Anatoliy Senyshyn, Clarina dela Cruz, Wei Yi, Jia-Wei Mei, Zi Yang Meng, Youguo Shi, and Shiliang Li, “Effect of Zn doping on the antiferromagnetism in kagome $\text{Cu}_{4-x}\text{Zn}_x(\text{OH})_6\text{FBr}$,” *Phys. Rev. B* **98**, 155127 (2018).
- [12] K. Kitagawa, T. Takayama, Y. Matsumoto, A. Kato, R. Takano, Y. Kishimoto, S. Bette, R. Dinnebier, G. Jackeli, and H. Takagi, “A spin-orbital-entangled quantum liquid on a honeycomb lattice,” *Nature* **554**, 341 (2018).
- [13] Alexei Kitaev, “Anyons in an exactly solved model and beyond,” *Annals of Physics* **321**, 2 – 111 (2006).
- [14] X.G. Wen, *Quantum Field Theory of Many-Body Systems: From the Origin of Sound to an Origin of Light and Electrons*, Oxford Graduate Texts (OUP Oxford, 2004).
- [15] Alexei Kitaev and John Preskill, “Topological Entanglement Entropy,” *Phys. Rev. Lett.* **96**, 110404 (2006).
- [16] Michael Levin and Xiao-Gang Wen, “Detecting Topological Order in a Ground State Wave Function,” *Phys. Rev. Lett.* **96**, 110405 (2006).
- [17] Xiao-Gang Wen, “Colloquium: Zoo of quantum-topological phases of matter,” *Rev. Mod. Phys.* **89**, 041004 (2017).
- [18] Xiao-Gang Wen, “Choreographed entanglement dances: Topological states of quantum matter,” *Science* **363** (2019), [10.1126/science.aal3099](https://doi.org/10.1126/science.aal3099).
- [19] G. Jackeli and G. Khaliullin, “Mott Insulators in the Strong Spin-Orbit Coupling Limit: From Heisenberg to a Quantum Compass and Kitaev Models,” *Phys. Rev. Lett.* **102**, 017205 (2009).
- [20] Jiří Chaloupka, George Jackeli, and Giniyat Khaliullin, “Kitaev-Heisenberg Model on a Honeycomb Lattice: Possible Exotic Phases in Iridium Oxides A_2IrO_3 ,” *Phys. Rev. Lett.* **105**, 027204 (2010).
- [21] Hidenori Takagi, Tomohiro Takayama, George Jackeli, Giniyat Khaliullin, and Stephen E. Nagler, “Concept

- and realization of kitaev quantum spin liquids,” *Nature Reviews Physics* **1**, 264–280 (2019).
- [22] S. K. Choi, R. Coldea, A. N. Kolmogorov, T. Lancaster, I. I. Mazin, S. J. Blundell, P. G. Radaelli, Yogesh Singh, P. Gegenwart, K. R. Choi, S.-W. Cheong, P. J. Baker, C. Stock, and J. Taylor, “Spin Waves and Revised Crystal Structure of Honeycomb Iridate Na_2IrO_3 ,” *Phys. Rev. Lett.* **108**, 127204 (2012).
- [23] Yogesh Singh, S. Manni, J. Reuther, T. Berlijn, R. Thomale, W. Ku, S. Trebst, and P. Gegenwart, “Relevance of the Heisenberg-Kitaev Model for the Honeycomb Lattice Iridates A_2IrO_3 ,” *Phys. Rev. Lett.* **108**, 127203 (2012).
- [24] Sae Hwan Chun, Jong-Woo Kim, Jungho Kim, H. Zheng, Constantinos C. Stoumpos, C. D. Malliakas, J. F. Mitchell, Kavita Mehlawat, Yogesh Singh, Y. Choi, T. Gog, A. Al-Zein, M. Moretti Sala, M. Krisch, J. Chaloupka, G. Jackeli, G. Khaliullin, and B. J. Kim, “Direct evidence for dominant bond-directional interactions in a honeycomb lattice iridate Na_2IrO_3 ,” *Nature Physics* **11**, 462 (2015).
- [25] K. W. Plumb, J. P. Clancy, L. J. Sandilands, V. Vijay Shankar, Y. F. Hu, K. S. Burch, Hae-Young Kee, and Young-June Kim, “ α - RuCl_3 : A spin-orbit assisted Mott insulator on a honeycomb lattice,” *Phys. Rev. B* **90**, 041112 (2014).
- [26] R. D. Johnson, S. C. Williams, A. A. Haghighirad, J. Singleton, V. Zapf, P. Manuel, I. I. Mazin, Y. Li, H. O. Jeschke, R. Valentí, and R. Coldea, “Monoclinic crystal structure of α - RuCl_3 and the zigzag antiferromagnetic ground state,” *Phys. Rev. B* **92**, 235119 (2015).
- [27] S. C. Williams, R. D. Johnson, F. Freund, Sungkyun Choi, A. Jesche, I. Kimchi, S. Manni, A. Bombardi, P. Manuel, P. Gegenwart, and R. Coldea, “Incommensurate counterrotating magnetic order stabilized by Kitaev interactions in the layered honeycomb α - Li_2IrO_3 ,” *Phys. Rev. B* **93**, 195158 (2016).
- [28] Y. Kasahara, T. Ohnishi, Y. Mizukami, O. Tanaka, Sixiao Ma, K. Sugii, N. Kurita, H. Tanaka, J. Nasu, Y. Motome, T. Shibauchi, and Y. Matsuda, “Majorana quantization and half-integer thermal quantum hall effect in a kitaev spin liquid,” *Nature* **559**, 227–231 (2018).
- [29] Y. J. Yu, Y. Xu, K. J. Ran, J. M. Ni, Y. Y. Huang, J. H. Wang, J. S. Wen, and S. Y. Li, “Ultralow-Temperature Thermal Conductivity of the Kitaev Honeycomb Magnet α - RuCl_3 across the Field-Induced Phase Transition,” *Phys. Rev. Lett.* **120**, 067202 (2018).
- [30] V. Hermann, M. Altmeyer, J. Ebad-Allah, F. Freund, A. Jesche, A. A. Tsirlin, M. Hanfland, P. Gegenwart, I. I. Mazin, D. I. Khomskii, R. Valentí, and C. A. Kuntscher, “Competition between spin-orbit coupling, magnetism, and dimerization in the honeycomb iridates: α - Li_2IrO_3 under pressure,” *Phys. Rev. B* **97**, 020104 (2018).
- [31] Gaomin Li, Xiaobin Chen, Yuan Gan, Fenglei Li, Mingqi Yan, Fan Ye, Shenghai Pei, Yujun Zhang, Le Wang, Huimin Su, Junfeng Dai, Yuanzhen Chen, Youguo Shi, Xinwei Wang, Liyuan Zhang, Shanmin Wang, Dapeng Yu, Fei Ye, Jia-Wei Mei, and Mingyuan Huang, “Raman spectroscopy evidence for dimerization and Mott collapse in α - RuCl_3 under pressures,” *Phys. Rev. Materials* **3**, 023601 (2019).
- [32] Gaomin Li, *et. al.*, to be submitted.
- [33] Sebastian Bette, Tomohiro Takayama, Kentaro Kitagawa, Riku Takano, Hidenori Takagi, and Robert E. Nebier, “Solution of the heavily stacking faulted crystal structure of the honeycomb iridate $\text{H}_3\text{LiIr}_2\text{O}_6$,” *Dalton Transactions* **46**, 15216–15227 (2017).
- [34] Kevin Slagle, Wonjune Choi, Li Ern Chern, and Yong Baek Kim, “Theory of a quantum spin liquid in the hydrogen-intercalated honeycomb iridate $\text{H}_3\text{LiIr}_2\text{O}_6$,” *Phys. Rev. B* **97**, 115159 (2018).
- [35] Ravi Yadav, Rajyavardhan Ray, Mohamed S Eldeeb, Satoshi Nishimoto, Liviu Hozoi, and Jeroen van den Brink, “Strong Effect of Hydrogen Order on Magnetic Kitaev Interactions in $\text{H}_3\text{LiIr}_2\text{O}_6$,” *Physical review letters* **121**, 197203 (2018).
- [36] Ying Li, Stephen M Winter, and Roser Valentí, “Role of Hydrogen in the Spin-Orbital-Entangled Quantum Liquid Candidate $\text{H}_3\text{LiIr}_2\text{O}_6$,” *Physical review letters* **121**, 247202 (2018).
- [37] Shuai Wang, Long Zhang, and Fa Wang, “Possible Quantum Paraelectric State in Kitaev Spin Liquid Candidate $\text{H}_3\text{LiIr}_2\text{O}_6$,” *arXiv e-prints* (2018), [arXiv:1807.03092](https://arxiv.org/abs/1807.03092) [[cond-mat.str-el](https://arxiv.org/abs/1807.03092)].
- [38] Johannes Knolle, Roderich Moessner, and Natalia B. Perkins, “Bond-Disordered Spin Liquid and the Honeycomb Iridate $\text{H}_3\text{LiIr}_2\text{O}_6$: Abundant Low-Energy Density of States from Random Majorana Hopping,” *Phys. Rev. Lett.* **122**, 047202 (2019).
- [39] Tôru Moriya, “Theory of Absorption and Scattering of Light by Magnetic Crystals,” *Journal of Applied Physics* **39**, 1042–1049 (1968).
- [40] P. A. Fleury and R. Loudon, “Scattering of light by one- and two-magnon excitations,” *Phys. Rev.* **166**, 514–530 (1968).
- [41] Peter Lemmens, Gernot Güntherodt, and Claudius Gros, “Magnetic light scattering in low-dimensional quantum spin systems,” *Physics Reports* **375**, 1 – 103 (2003).
- [42] Luke J. Sandilands, Yao Tian, Kemp W. Plumb, Young-June Kim, and Kenneth S. Burch, “Scattering Continuum and Possible Fractionalized Excitations in α - RuCl_3 ,” *Phys. Rev. Lett.* **114**, 147201 (2015).
- [43] A. Glamazda, P. Lemmens, S. H. Do, Y. S. Choi, and K. Y. Choi, “Raman spectroscopic signature of fractionalized excitations in the harmonic-honeycomb iridates β - and γ - Li_2IrO_3 ,” *Nature Communications* **7**, 12286 (2016).
- [44] A. Glamazda, P. Lemmens, S.-H. Do, Y. S. Kwon, and K.-Y. Choi, “Relation between Kitaev magnetism and structure in α - RuCl_3 ,” *Phys. Rev. B* **95**, 174429 (2017).
- [45] J. Knolle, D. L. Kovrizhin, J. T. Chalker, and R. Moessner, “Dynamics of a two-dimensional quantum spin liquid: Signatures of emergent majorana fermions and fluxes,” *Phys. Rev. Lett.* **112**, 207203 (2014).
- [46] F. Freund, S. C. Williams, R. D. Johnson, R. Coldea, P. Gegenwart, and A. Jesche, “Single crystal growth from separated educts and its application to lithium transition-metal oxides,” *Scientific Reports* **6**, 35362 (2016).
- [47] <https://srdata.nist.gov/xps/Default.aspx>.
- [48] J. Knolle, Gia-Wei Chern, D. L. Kovrizhin, R. Moessner, and N. B. Perkins, “Raman Scattering Signatures of Kitaev Spin Liquids in A_2IrO_3 Iridates with $\text{A} = \text{Na}$ or Li ,” *Phys. Rev. Lett.* **113**, 187201 (2014).
- [49] J. Nasu, J. Knolle, D. L. Kovrizhin, Y. Motome, and R. Moessner, “Fermionic response from fractionalization in an insulating two-dimensional magnet,” *Nature Physics* **12**, 912 (2016).